

Superconductivity and Frozen Electronic States at the (111) $\text{LaAlO}_3/\text{SrTiO}_3$ Interface

S. Davis,^{1,*} Z. Huang,^{2,3} K. Han,^{2,3} Ariando,^{2,3,4} T. Venkatesan,^{4,5,6,7,8} and V. Chandrasekhar^{1,†}

¹Graduate Program in Applied Physics and Department of Physics and Astronomy,
Northwestern University, 2145 Sheridan Road, Evanston, IL 60208, USA

²NUSNNI-Nanocore, National University of Singapore 117411, Singapore

³Department of Physics, National University of Singapore 117551, Singapore

⁴NUS Graduate School for Integrative Sciences & Engineering,
National University of Singapore 117456, Singapore

⁵NUSNNI-NanoCore, National University of Singapore 117411, Singapore

⁶Department of Physics, National University of Singapore 117542, Singapore

⁷Department of Electrical and Computer Engineering,
National University of Singapore 117576, Singapore

⁸Department of Material Science and Engineering,
National University of Singapore 117575, Singapore

(Dated: April 6, 2017)

In spite of Anderson's theorem¹, disorder is known to affect superconductivity in conventional *s*-wave superconductors^{2–11}. In most superconductors, the degree of disorder is fixed during sample preparation. Here we report measurements of the superconducting properties of the two-dimensional gas that forms at the interface between LaAlO_3 (LAO) and SrTiO_3 (STO) in the (111) crystal orientation, a system that permits *in situ* tuning of carrier density and disorder by means of a back gate voltage V_g . Like the (001) oriented LAO/STO interface^{12–15}, superconductivity at the (111) LAO/STO interface can be tuned by V_g . In contrast to the (001) interface, superconductivity in these (111) samples is anisotropic, being different along different interface crystal directions, consistent with the strong anisotropy already observed in other transport properties at the (111) LAO/STO interface^{16,17}. In addition, we find that the (111) interface samples “remember” the backgate voltage V_F at which they are cooled at temperatures near the superconducting transition temperature T_c , even if V_g is subsequently changed at lower temperatures. The low energy scale and other characteristics of this memory effect (< 1 K) distinguish it from charge-trapping effects previously observed in (001) interface samples.

For most conventional superconductors, the presence of disorder decreases the superconducting transition temperature, T_c ^{2,3}. While the exact reason for this is still a subject of investigation, it is thought that localization effects coupled with enhanced Coulomb interactions resulting from the short elastic mean free path give rise to an inhomogeneous superconducting state with large amplitude and phase variations, even though the disorder may be uniform^{7–9}. In the limit of large disorder, the material may transition into an insulating state, the so-called superconductor-to-insulator transition (SIT)⁷.

In a few superconductors, increasing disorder increases T_c : perhaps the best-known example is Al, where the enhancement of T_c with disorder can be as large as a factor of 5^{4,5}. In this case, the enhancement in T_c is thought to be due to a modification of the electron-phonon interaction responsible for the attractive potential between quasiparticles.^{2,10,11}

A SIT has been observed in the (001) LAO/STO interfaces^{12–15}; unlike other thin films discussed above, the advantage of this two-dimensional (2D) system is that the system parameters can be changed by simply changing the voltage V_g on a gate, enabling tuning of the SIT with an *in situ* experimental handle. As we show below, the (111) LAO/STO interface devices also show a superconducting transition that can be tuned by V_g . Unlike the (001) LAO/STO devices, however, the superconducting characteristics are anisotropic, being different when measured along two mutually perpendicular crystal directions. This behavior complements the strong anisotropy that we have reported recently in other transport properties of the (111) interface, including the longitudinal resistance, Hall effect and quantum capacitance^{16,17}: as discussed there, the anisotropy is not due to the hexagonal symmetry of the (111) interface, microstructural effects or ferroelectric twin domains. More remarkably, both the normal and superconducting properties at temperatures $T \sim T_c$ and below strongly depend on the gate voltage V_F as the sample is cooled from ~ 4 K, even if V_g is subsequently changed at lower temperatures. This freezing effect is an indication of disorder that can be frozen in at very low temperatures in these structures by the application of a gate voltage, and which can be reversed by warming the sample to a freezing temperature $T_F \sim 1$ K, and is distinctly different in energy scale and qualitative response to V_g from the charge trapping behavior reported earlier in (001) LAO/STO interface samples^{14,18–20}.

The heterostructures used in this work consisted of 20 monolayers (ML) of LAO grown epitaxially on Ti termi-

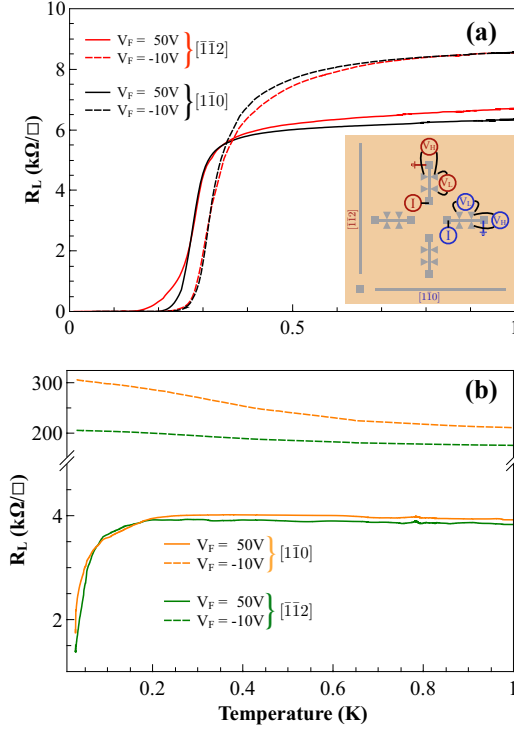


FIG. 1. **Resistance as a function of temperature with different freezing voltages V_F along two crystal directions.** The Ar/H₂ annealed samples (a) show full superconducting transitions. While the normal state resistance R_N is higher for $V_F = -10$ V, the superconducting transition temperature T_c is also higher. The O₂ annealed samples (b) do not go superconducting, but show hints of a superconducting transition for $V_F = 50$ V, and insulating behavior for $V_F = -10$ V, with strong anisotropy between the the $[\bar{1}\bar{1}2]$ and $[1\bar{1}0]$ crystal directions in the latter. Inset in (a) is a schematic of the Hall bars on each sample chip, which shows the measurement configuration.

nated (111) STO substrates by pulsed laser deposition. Details of the film synthesis can be found in *Methods*. On each 5 mm×5 mm chip, 4 Hall bars ($600\ \mu\text{m} \times 100\ \mu\text{m}$) were fabricated using a combination of photolithography and Ar ion milling such that two of the Hall bars were oriented along the $[\bar{1}\bar{1}2]$ surface crystal direction, and the remaining two were oriented along the $[1\bar{1}0]$ crystal direction, as shown in the inset to Fig. 1(a). Chips were then exposed to different post-growth annealing processes to change their global carrier densities. Half of the devices were annealed in an O₂ atmosphere and the other half in a Ar/H₂ atmosphere (see *Methods*). Annealing in an O₂ environment reduces the number of oxygen vacancies and hence reduces the carrier concentration, while annealing in Ar/H₂ increases the oxygen vacancy concentration and hence increases the carrier concentration¹⁷. A total of 10 Hall bars on three different chips were measured; here we

report data on the four Hall bars for which we have the most comprehensive data.

In (111) interface structures, the transport characteristics (longitudinal resistance, Hall coefficient, and quantum capacitance) are strongly anisotropic^{16,17}, being different along the $[\bar{1}\bar{1}2]$ and $[1\bar{1}0]$ directions, the anisotropy increasing with decreasing oxygen vacancy concentration and more negative V_G ¹⁷. As we show below, the superconducting characteristics are also anisotropic. Figure 1(a) shows the superconducting transition of a Ar/H₂ annealed sample with back gate ‘freezing’ voltages $V_F = -10$ V and $V_F = 50$ V applied as the sample was cooled through the transition. To maintain a uniform protocol for all data taken, V_F was applied at a temperature of 4.4 K before cooling down to 30 mK, unless otherwise noted. V_G was then repeatedly cycled between ± 100 V to obtain reproducible curves (see Supplementary Information) before the data reported here were taken.

The data discussed here are for two freezing voltages $V_F = -10$ V and $V_F = 50$ V for which we have taken the most extensive data. Data for other voltages (e.g., $V_F = 0$ V) follow the expected trend (see Supplementary Information). The Ar/H₂ annealed samples showed a superconducting transition, with V_F affecting both the normal state resistance R_N and the superconducting transition T_c . As expected from our previous work^{16,17}, the Ar/H₂ annealed samples, with a larger number of oxygen vacancies, are not strongly anisotropic. The O₂ annealed samples did not go fully superconducting: there is a hint of a superconducting transition for $V_F = 50$ V, while insulating behavior is seen for $V_F = -10$ V, with clear anisotropy in resistance between the two crystal directions (a much stronger anisotropy is observed at lower gate voltages^{16,17}). A similar dependence of the superconducting properties on gate voltage has been reported in (001) LAO/STO structures, and is ascribed to electrostatic doping of the electron gas. We show below that part of the difference in the (111) LAO/STO devices is due to disordered trapped states frozen in by the application of a gate voltage at higher temperatures.

The difference between electrostatic doping and frozen disorder can be seen clearly in the nonlinear differential resistance dV/dI as a function of dc current I_{dc} and gate voltage V_g at temperatures far below T_c , shown in Fig. 2 for the Ar/H₂ annealed samples. As expected, the critical current I_c varies with V_g , being in general smaller for more negative V_g . This is the effect of electrostatic doping with V_g , similar to that observed previously in the (001) LAO/STO samples¹⁵. However, the most striking feature of this data is that the current-voltage characteristics also depend on the gate voltage V_F at which the samples were cooled, even though V_g is changed over the same range. The difference is persistent: as noted above, data were taken after the gate voltage had been swept repeatedly between ± 100 V at 30 mK; the sample remembers the voltage V_F at which it was cooled.

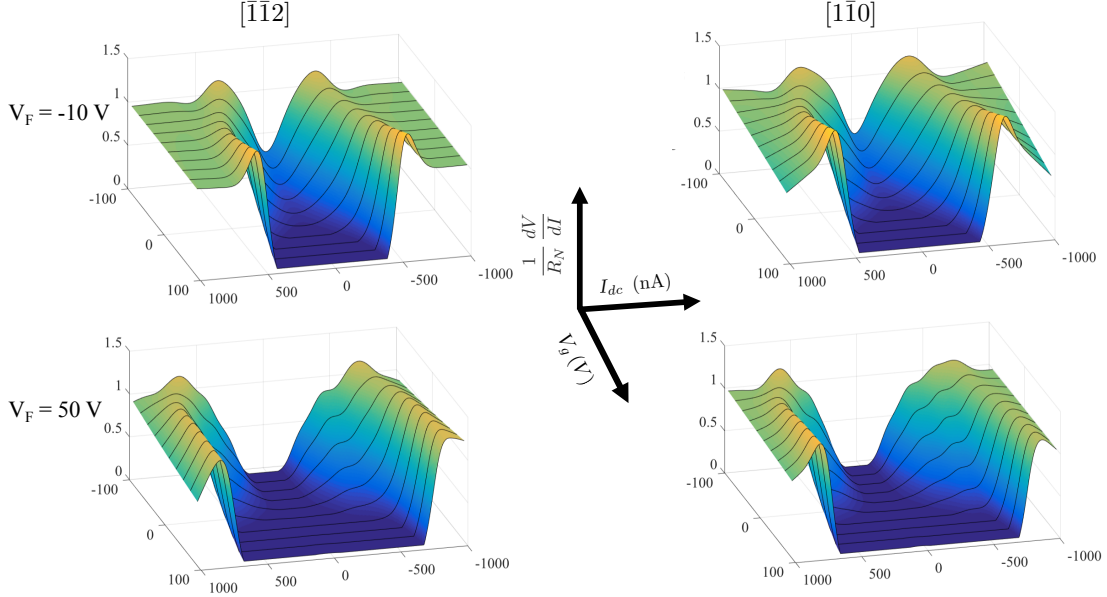


FIG. 2. **Differential resistance of the Ar/H₂ annealed samples at 30 mK, for $V_F = -10$ V and $V_F = 50$ V.** The critical current I_c varies with V_g , a consequence of electrostatic doping by the gate, but is also a function of the freezing voltage V_F applied while cooling through the superconducting transition: in general, I_c is larger for $V_F = 50$ V in comparison to $V_F = -10$ V. For the Ar/H₂ annealed devices, there is relatively little anisotropy between the two crystal directions. Due to the large variation in R_N with V_g , the curves here and in Fig. 3 are normalized to the value of dV/dI at ± 1 μ A.

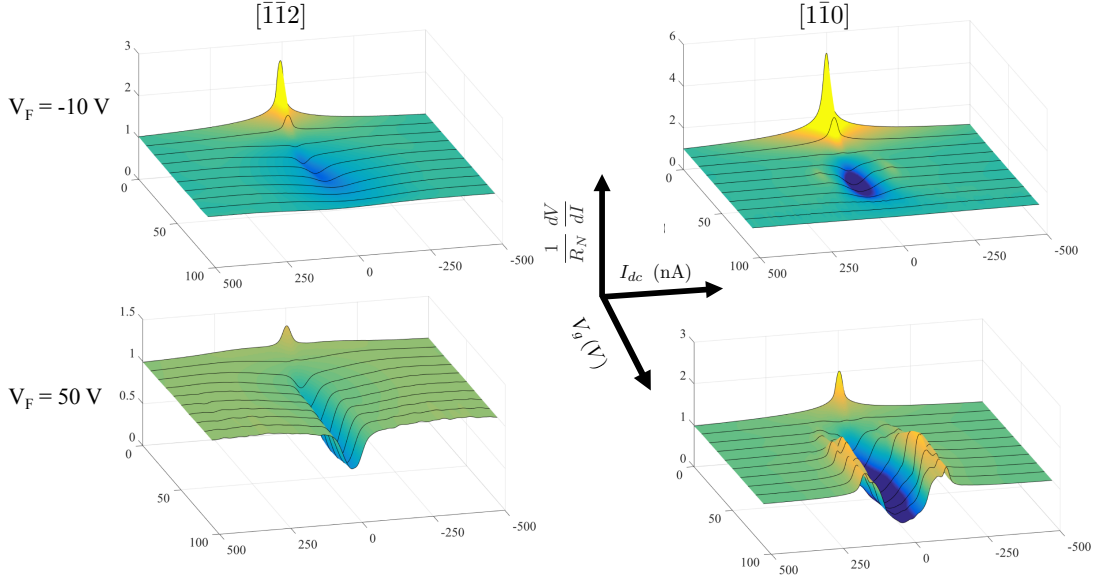


FIG. 3. **Differential resistance of the O₂ annealed samples at 30 mK, for $V_F = -10$ V and $V_F = 50$ V.** While the O₂ annealed samples do not go fully superconducting, there is clear evidence for incipient superconductivity in the current-voltage characteristics, even for $V_F = -10$ V, for which the resistance increases with decreasing temperature (Fig. 1(b)). As with the Ar/H₂ annealed samples (Fig. 2), the superconducting characteristics change with V_g , a consequence of electrostatic doping, but also are a function of the voltage V_F at which they are cooled. For the O₂ annealed samples, the superconducting characteristics are also highly anisotropic, being very different along the two crystal directions, as has been reported earlier for other transport properties^{16,17}. Clear evidence for a maximum in superconducting properties as a function of V_g (the superconducting ‘dome’) can also be seen.

Figure 3 shows similar data for the O₂ annealed samples. Here, the samples do not go completely superconducting, although a dip in the differential resistance can clearly be seen over a certain range of V_g , mimicking the dome observed in (001) LAO/STO samples^{14,15}. Even so, the freezing effect is quite clear: in both crystal directions, the drop in differential resistance near zero bias along both crystal directions is much larger for $V_F = 50$ V than for $V_F = -10$ V. We note that the O₂ annealed samples are also strongly anisotropic, which can be seen most strikingly in the data in Fig. for $V_F = 50$ V. (The anisotropy in the Ar/H₂ annealed samples is much weaker, but still present.)

A different representation of the data for the Ar/H₂ annealed samples in Fig. 2 is given in Figs. 4(a) and (b), which show I_c and the normal state resistance R_N as a function of V_g for the Ar/H₂ annealed samples. In general, R_N increases rapidly with decreasing V_g , as expected, but the sharp upturn in R_N occurs at larger V_g for $V_F = -10$ V in comparison to $V_F = 50$ V. I_c shows a broad maximum, in effect, a saturation, at positive V_g , occurring at around $V_g \sim 0$ V for $V_F = 50$ V, and $V_g \geq 100$ V for $V_F = -10$ V. However, the I_c 's for $V_F = -10$ V are approximately a factor of 2 smaller than those for $V_F = 50$ V. Thus, setting a gate voltage $V_F = -10$ V as the sample is cooled through its transition results in lower critical currents over the entire gate voltage range in comparison to $V_F = 50$ V. However, T_c shows a different trend (Fig. 4(c)). T_c is lower for $V_F = -10$ V than for $V_F = 50$ V for $V_g \leq -60$ V, but uniformly larger above this value. This trend of an increase of T_c coupled with a decrease in I_c has also been observed in Al films^{4,5}, and has been associated there with a modification with disorder of the attractive electron-phonon interaction responsible for superconductivity.^{10,11}

From these data, it is evident that applying a back-gate voltage V_F as the sample is cooled through its transition freezes in a specific configuration that influences the normal and superconducting state properties at very low temperatures, even if V_g is subsequently swept. The configuration is stable in time over a scale of weeks, and robust against changes in I_{dc} and magnetic field in addition to V_g , so long as the temperature is not raised above a certain freezing temperature T_F . In order to determine T_F , we cooled the devices down from 4.4 K to a target temperature with gate voltages of either $V_F = -10$ V or $V_F = 50$ V applied, and then measured the resistance as a function of V_g . After each resistance measurement, the sample was warmed to 4.4 K before another measurement was made. These traces for 4 target temperatures of 30 mK, 470 mK, 675 mK and 1.2 K are shown in Fig. 5. For simplicity, we have shown data for only the Ar/H₂ annealed devices in the $[\bar{1}\bar{1}2]$ crystal direction: Data for the other crystal direction are shown in the Supplementary Information. At 1.2 K and 675 mK, there is only a small difference in the resistance

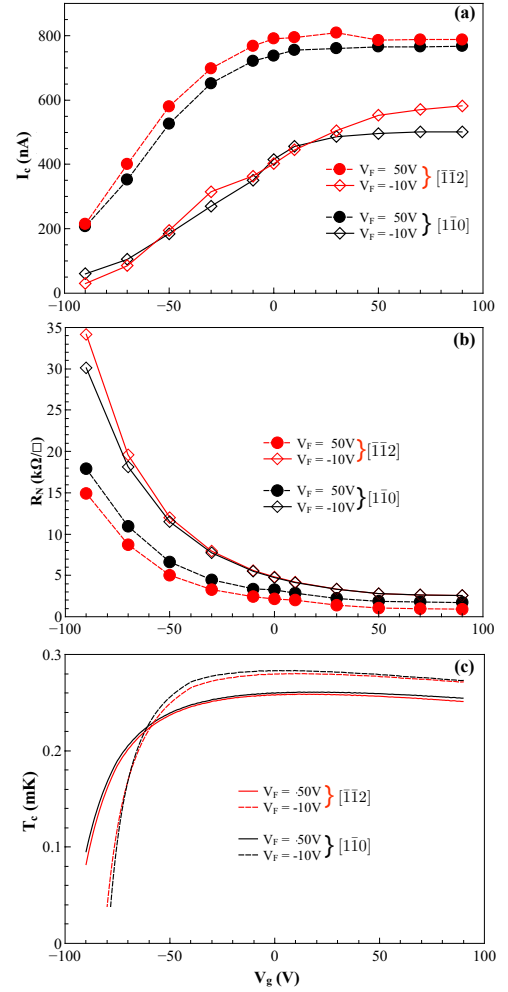


FIG. 4. **Superconducting properties of the Ar/H₂ annealed samples for different freezing voltages.** Critical current I_c (a), normal state resistance (b) for the Ar/H₂ annealed samples for freezing voltages $V_F = -10$ V and $V_F = 50$ V, for both the $[\bar{1}\bar{1}2]$ and $[\bar{1}\bar{1}0]$ crystal directions, taken from Fig. 2. Since the data show multiple peaks, I_c is defined to be the value of I_{dc} at which the slope of dV/dI vs I_{dc} is a maximum ($d^3V/dI^3 = 0$). R_N is defined as the value of dV/dI at $I_{dc} \pm 1$ μ A. (c) Critical temperature T_c as a function of V_g , measured using feedback techniques by biasing the device at the foot of the superconducting transition while sweeping V_g (see *Methods*).

as a function of V_g . At 470 mK, the difference is much larger, almost a factor of 5 at negative V_g . Finally, at 30 mK, the difference is almost an order of magnitude at negative V_g (the sample is superconducting for $V_g > -40$ V at this temperature). Thus the temperature at which the configuration is frozen in is $T_F \sim 1$ K.

We now come to the question of the origin of this effect. In (001) interface samples, the resistance at low temperature depends on the history of how V_g is swept after first

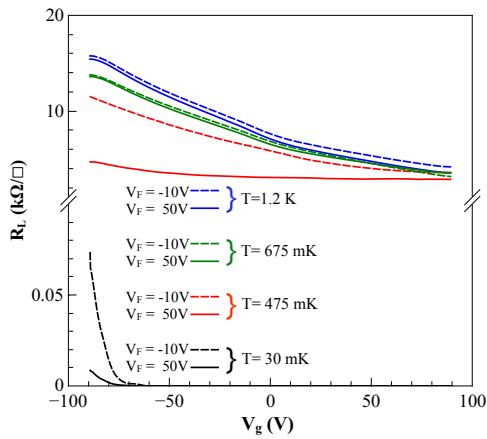


FIG. 5. **Onset of the freezing transition.** Resistance of the Ar/H₂ annealed samples in the $[\bar{1}\bar{1}2]$ crystal orientation as a function of V_g after cooling from 4.4 K to the target temperatures noted with gate voltages $V_F = -10$ V and $V_F = 50$ V applied. As the resistance is hysteretic with V_g , the average of the upsweep and downsweep traces as a function of V_g is shown in each case. Differences between the curves for the two freezing temperatures show up only below 600-700 mK, showing that the freezing temperature T_F is of order ~ 0.6 K.

cooling the sample down from room temperature, eventually settling into a hysteretic but reproducible behavior as a function of V_g . This has been ascribed to an irreversible change in the occupation of charge states near the interface that can only be reset by warming to room temperature, indicating that the relevant energy scales for population or depopulation of these charge states are of that order (~ 25 meV). We also observe a similar initial, irreproducible, history dependence of the properties in the (111) interface samples on first cooling down from room temperature, after which the properties as a function of V_g become hysteretic but reproducible. However, the freezing effects in the (111) interface samples reported here are different, in that different values and V_g dependences of I_C , R_N and T_C can be stabilized at very low temperature depending on the freezing voltage V_F without introducing new irreproducible dependences at these temperatures. Furthermore, these frozen state sets/resets at a much lower energy scale, ~ 1 K. It may be possible that the freezing effect is associated with other trapped states with much lower energy scales. From Fig. 4, it appears that shifting the $V_F = 50$ V curves towards positive V_g would roughly align the curves for the two different freezing temperatures, although the shifts would be different for R_N , I_C , and T_C . However, it is clear that even with shifting one of the curves with V_g , the superconducting properties cannot be made to align, as the saturation values of I_C and R_N for large V_g for the two freezing temperatures are quite different. Consequently, it is clear that the effects that we observe are not solely

due to residual electric fields due to trapped charges, at least with regard to the superconducting properties: the effects we observe, particularly the increase in T_C for $V_F = -10$ V, similar to what is observed in Al films, suggests that increased disorder due to the trapped charges may be important. If the freezing of charged trap states is indeed responsible for the freezing effect we observe, at 1 K, one would need to understand the very low energy scales of these states. Uncovering the origin of these low energy scales will require further experimental and theoretical work.

METHODS

The 20 monolayer (ML) (111) LAO/STO interface samples reported on in this study were prepared by pulsed laser deposition using a KrF laser ($\lambda = 248$ nm). A LAO single crystal target was used for deposition, and the laser repetition was kept at 1 Hz, laser fluence at 1.8 J/cm², growth temperature at 650 C, and oxygen pressure at 1 mTorr. The deposition was monitored via *in situ* reflection high energy electron diffraction (RHEED). Hall bars were then fabricated using photolithography to define an etch mask to protect the Hall bars during the subsequent argon ion milling. The argon ion milling etched the unprotected areas to the bare STO, leaving the LAO on top of the Hall bars. A final photolithography step deposited a Au film on the electrical contacts to enable visual location of the contacts for wire-bonding. Additionally, Au was deposited on the etched bare STO, which enabled us to confirm that the bare STO did not become conducting after the ion milling process or subsequent annealing steps.

The crystal orientation of the Hall bars shown in inset of Fig. 1(a) of the manuscript were determined via x-ray diffraction utilizing a Photonic Science Laue X-ray camera. The sample was mounted on a goniometer stage for precise angular alignment. The images were fit using the commercial PSL software provided with the camera, which allowed simultaneous determination of both Hall bar orientations on the substrate, as marked in the inset of Fig. 1(a) of the main manuscript. The samples were then subjected to post growth surface treatments to change the oxygen vacancy concentration at the interface. Four of the devices were subjected to O₂ annealing and other six devices were subjected to Ar/H₂ annealing. The exact annealing processes are described in Ref. 17. The samples were cooled to millikelvin temperatures using both an Oxford MX100 and Kelvinox 300 dilution refrigerator. To measure the transport characteristics of the samples we utilized custom home-built amplifiers and high impedance current sources in conjunction with traditional lock-in techniques, allowing for measurement of samples impedances of up to a GΩ. Further information about the feedback measurements used to measure

T_c continuously as a function of V_g can be found in the Supplementary information.

-
- * samueldavis2016@u.northwestern.edu
† v-chandrasekhar@northwestern.edu
- ¹ P. W. Anderson, 'Theory of Dirty Superconductors,' J. Phys. Chem. Solids **11**, 26-30 (1959).
 - ² S. Bose, P. Raychaudhuri, R. Banerjee, P. Vasa, & P. Ayyub, 'Mechanism of the Size Dependence of the Superconducting Transition of Nanostructured Nb,' Phys. Rev. Lett. **95**, 147003 (2005).
 - ³ S. Matsuo, H. Sugiura, & S. Noguchi, 'Superconducting Transition Temperature of Aluminum, Indium, and Lead Fine Particles,' J. Low Temp. Phys. **15**, 5 (1974).
 - ⁴ B. Abeles, R. W. Cohen, and G. W. Cullen, 'Enhancement of Superconductivity in Metal Films,' Phys. Rev. Lett. **17**, 12 (1966).
 - ⁵ M. Nittmann, P. Ziemann, W. Buckel, & G. Linker, 'Dependence of the Superconducting Transition Temperature of Quench-Condensed Aluminium-Films on the Oxygen Content,' Z. Phys. B -Cond. Matter **41**, 205-209 (1981).
 - ⁶ M. Mondal, M. Chand, A. Kamlapure, J. Jesudasan, V. C. Bagwe, S. Kumar, G. Saraswat, V. Tripathi, & P. Raychaudhuri, 'Phase Diagram and Upper Critical Field of Homogeneously Disordered Epitaxial 3-Dimensional NbN Films,' J. Supercond. Nov. Magn. **24**, 341-344 (2011).
 - ⁷ N. Markovic, C. Christiansen, A. M. Mack, W. H. Huber, and A. M. Goldman, 'Superconductor-insulator transition in two dimensions,' Phys. Rev. B **60**, 6 (1999).
 - ⁸ E. Shimshoni, A. Auerbach, and A. Kapitulnik, 'Transport through Quantum Melts,' Phys. Rev. Lett. **80**, 15 (1998).
 - ⁹ A. Kamlapure, T. Das, S. C. Ganguli, J. B. Parmar, S. Bhattacharyya, & P. Raychaudhuri, 'Emergence of nanoscale inhomogeneity in the superconducting state of a homogeneously disordered conventional superconductor,' Sci. Rep. **3**, 2979 (2013).
 - ¹⁰ P. G. De Gennes, 'Boundary Effects in Superconductors,' Rev. Mod. Phys. **36**, 225 (1964).
 - ¹¹ J. W. Garland, K. H. Bennemann, and F. M. Mueller, 'Effect of Lattice Disorder on the Superconducting Transition Temperature,' Phys. Rev. Lett. **21**, 1315
 - ¹² S. Thiel, G. Hammerl, A. Schmehl, C.W. Schneider and J. Mannhart, 'Tunable Quasi-Two-Dimensional Electron Gases in Oxide Heterostructures,' *Science* **313**, 1942 (2006).
 - ¹³ N. Reyren, S. Gariglio, A. D. Caviglia, D. Jaccard, T. Schneider, and J.-M. Triscone 'Anisotropy of the superconducting transport properties of the LaAlO₃/SrTiO₃ interface,' *Appl. Phys. Letters* **94**, 11 (2009).
 - ¹⁴ A. D. Caviglia, S. Gariglio, N. Reyren, D. Jaccard, T. Schneider, M. Gabay, S. Thiel, G. Hammerl, J. Mannhart & J.-M. Triscone, 'Electric field control of the LaAlO₃/SrTiO₃ interface ground state,' *Nature* **456**, 624 (2008).
 - ¹⁵ D. A. Dikin, M. Mehta, C. W. Bark, C. M. Folkman, C. B. Eom, and V. Chandrasekhar, 'Coexistence of Superconductivity and Ferromagnetism in Two Dimensions,' *Phys.Rev.Lett.* **107**, 056802 (2011).
 - ¹⁶ S. K. Davis, Z. Huang, K. Han, Ariando, T. Venkatesan, V. Chandrasekhar, 'Anisotropic, Multi-carrier Transport at the (111) LaAlO₃/SrTiO₃ Interface ,' Phys. Rev. B **95**, 035127 (2017)
 - ¹⁷ S. K. Davis, Z. Huang, K. Han, Ariando, T. Venkatesan, V. Chandrasekhar, 'Electrical Transport Anisotropy Controlled by Oxygen Vacancy Concentration in (111) LaAlO₃/SrTiO₃ Interface Structures,' Adv. Mater. Interfaces, 1600830 (2017).
 - ¹⁸ Z.Q. Liu, D.P. Leusink, X. Wang, W.M. Lu, K. Gopinadhan, A. Annadi, Y. L. Zhao, X.H. Huang, S.W. Zeng, Z. Huang, A. Srivastava, S. Dhar, T. Venkatesan, and Ariando, 'Metal-Insulator Transition in SrTiO_{3-x} Thin Films Induced by Frozen-Out Carriers', Phys. Rev. Lett. **107**, 146802 (2011).
 - ¹⁹ C. Bell, S. Harashima, Y. Kozuka, M. Kim, B. G. Kim, Y. Hikita, and H. Y. Hwang, 'Dominant Mobility Modulation by the Electric Field Effect at the LaAlO₃/SrTiO₃ Interface,' *Phys.Rev.Lett.* **103**, 056802 (2009)
 - ²⁰ J. Biscaras, S. Hurand, C. Feuillet-Palma, A. Rastogi, R. C. Budhani, N. Reyren, E. Lesne, J. Lesueur and N. Bergeal, 'Limit of the electrostatic doping in two-dimensional electron gases of LaXO₃(X=Al,Ti)/SrTiO₃,' Sci. Rep. **4**, 6788 (2014)